Electronic Structure and Localized States at Carbon Nanotube Tips

D. L. Carroll,* P. Redlich, and P. M. Ajayan†
Max-Planck-Institut für Metallforschung, Seestraße 92, 70174 Stuttgart, Germany

J. C. Charlier,‡ X. Blase,§ A. De Vita, and R. Car
Institut Romand de Recherche Numerique en Physique des Materiaux IN-Ecublens, CH-1015 Lausanne, Switzerland
(Received 12 August 1996; revised manuscript received 25 November 1996)

Topology related changes in the local density of states near the ends of closed carbon nanotubes are investigated using spatially resolved scanning tunneling spectroscopy and tight binding calculations. Sharp resonant valence band states are observed in the experiment at the tube ends, dominating the valence band edge and filling the band gap. Calculations show that the strength and position of these states with respect to the Fermi level depend sensitively on the relative positions of pentagons and their degree of confinement at the tube ends. [S0031-9007(97)02881-0]

PACS numbers: 73.20.Dx, 61.16.Ch, 61.48.+c

Carbon nanotubes constitute the link between large carbon fibers used as mechanical reinforcements in composites and molecular wires that could lead to ideal electrical connectors in future technology [1]. Two general categories of nanotubes exist presently. Singlewalled nanotubes [2] composed of single graphene sheets wrapped into cylinders with a narrow size distribution of 1–2 nm diameter. Multiwalled nanotubes [3] are larger (2–30 nm diameter) and are coaxial assemblies of graphene cylinders separated by approximately the c plane spacing (0.34 nm) of graphite. Both are in general microns in length and extremely stiff [4] with very high axial strength. The electrical properties of nanotubes are all the more interesting and have been treated extensively in many theoretical works [1]. Although most of the theoretical results have been obtained for singlewalled nanotubes, recent experiments on multiwalled structures confirm some of these results, indicating that nanotubes possess a rich variety of electronic structure with conductivities ranging from metallic to semiconducting [5]. The broad range in conductivities arises from the helicity of graphite lattice [3] in the nanotube structure and changes in the diameters of individual cylinders in the tube.

A more interesting structural feature occurs near the ends of all tubes from the closure of the graphene cylinders by the incorporation of topological defects such as pentagons in the hexagonal carbon lattice [6]. Complex end structures can arise, for instance conical shaped sharp tips, due to the way pentagons are distributed near the ends for full closure. It is suggested by theory [7] that the ends of the tubes should have different electronic structure due to the presence of topological defects though it has never been experimentally verified. Defect induced tip electronic structure is important for several reasons. For example, the field emission properties of nanotubes, which have been recently demonstrated [8], could be strongly influenced by the presence of localized resonant states [9].

Electrical properties measured by two and four probe measurements [5] and electronic structure of nanotubes of differing sizes studied by scanning tunneling microscopy (STM) and spectroscopy (STS) [1,10] have suggested a range of values for conductivities and band gaps (200 meV to 1.2 eV). However, the spatially resolved STS determinations of electronic properties are sensitive to ambient conditions, tube helicity, as well as where along the tube the measurements are made. For instance, if the density of defect states increases at the tube end, it can be expected that the electronic structure of the end would differ markedly from that elsewhere on the tube. This could be particularly well demonstrated in a conical shaped tube end where the pentagonal defects necessary for closure are concentrated at the apex of the cone. We have focused our experiments on tube end structures to see how their local density of states is affected by the incorporation of defects into the carbon network. The major question we address here is the following: How is the increasing defect concentration, at a tube tip, reflected in the local density of states (LDOS) of a nanotube. By coupling tight binding calculations performed on several tube tip morphologies and STS done on conical tube ends, we correlate sharp resonant features in LDOS with the presence of defects in the structure.

Carbon nanotubes were fabricated using the electric-arc-discharge method and characterized by electron microscopy as described elsewhere [11]. A dilute mixture of carbon nanotubes and ethanol was ultrasonically agitated, to separate tubes, and deposited on freshly cleaved highly oriented pyrolytic graphite (HOPG). The substrate was immediately mounted in a high vacuum prechamber and the ethanol pumped away to a pressure of 1.0×10^{-7} torr. The substrate was then introduced into ultrahigh vacuum (UHV) (base pressure of 5.0×10^{-10} torr) and loaded into a commercially available scanning tunneling microscopy (STM) (Park Scientific). All microscopy and spectroscopy were done using mechanically formed Pt-Ir tips.

While atomic resolution of the supporting substrate was always easily achieved, generally, atomic structure on the tube was not observed. This is attributed to small

tube-substrate interactions in UHV which lead to slight instabilities during imaging. Bias voltages greater than 0.5 V and setpoint of 1.5 nA could be used to pick the tubes up and position them anywhere on the substrate. With a tunneling voltage of 30 mV and setpoint of 0.5 nA, the tubes could be imaged repeatedly with no observed drift from image to image. Tunneling spectra were acquired using this setpoint at different positions along the tube, and compared to that of the HOPG substrate. Local differential conductivity (dI/dV) and local density of states were derived by the method of Feenstra [12].

Figure 1(a) shows two isolated tubes of approximately 10 nm each and Fig. 1(b) a conical shaped closure of the end of a 20 nm tube. The tubes in Fig. 1(a) terminate in hemispherical domes or polyhedra. The apex of the cone [Fig. 1(b)] should be close to a regular hemisphere with a diameter of ~2 nm. Figures 2(a) and 2(b) (schematic) show two models, described in detail later in the paper, for the cone termination which could possibly represent the structure shown in Fig. 1(b). From close examination of image cross section at the cone end, we find that Fig. 2(b) most closely represents the conical structure in our image.

The differential conductance and the LDOS for the isolated tubes in Fig. 1(a) is shown in Fig. 3 and compared to the HOPG substrate. From the conductance it is clear the carrier mobilities are lower (or the effective mass higher) in the tubes when compared to graphite. Further, a band gap opens up inducing semiconducting behavior

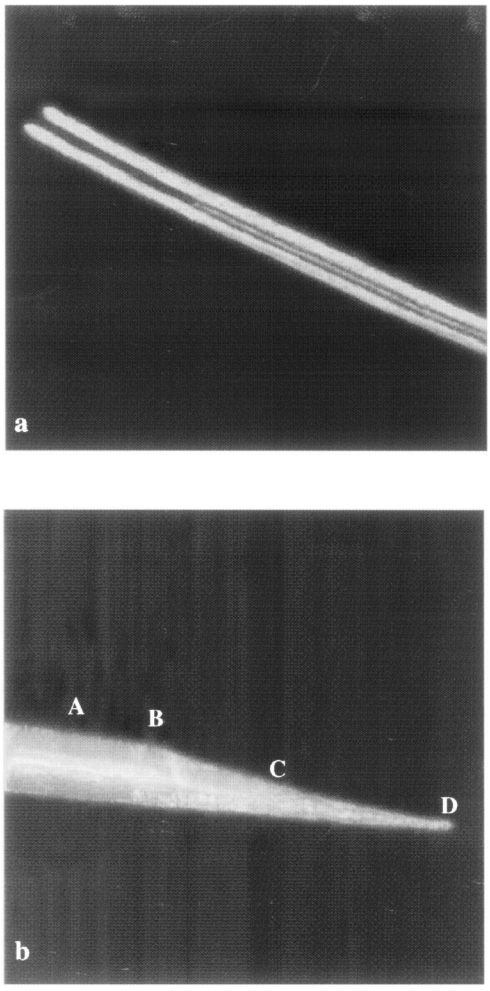

FIG. 1. STM images of carbon nanotubes acquired at constant current with a setpoint of 0.03 V and 0.25 nA. (a) 150 × 150 nm image of three tubes. The two larger tubes, from which spectra were collected, are approximately 10 nm in diameter. A much smaller third tube can be seen sandwiched between. (b) 100 × 100 nm image of a cone at the end of an approximately 20 nm diameter tube. The apex of the cone has a diameter of 2.0 nm. The white letters mark positions from where tunneling spectra were acquired.

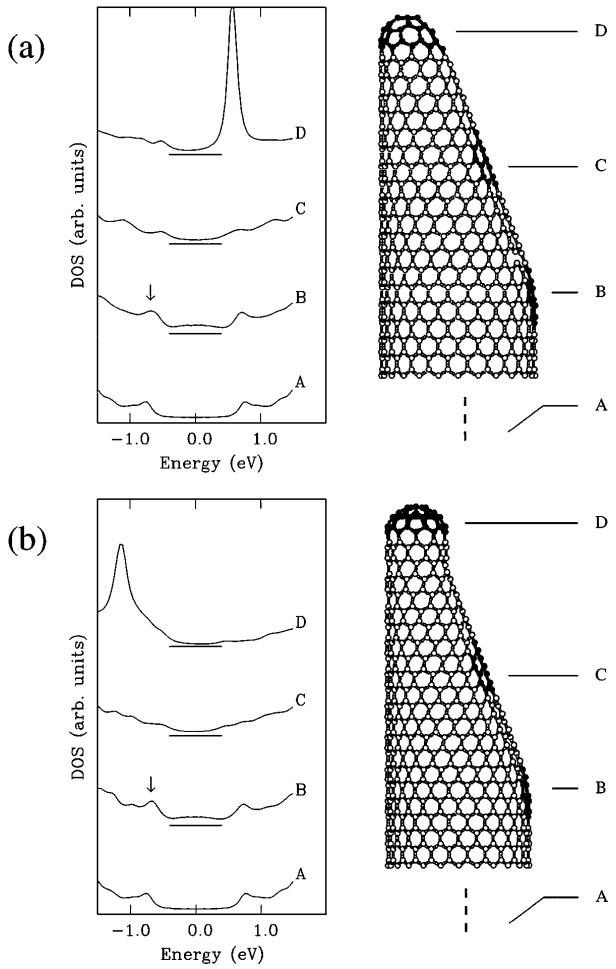

FIG. 2. Local densities of π-π^* electron states along a (24, 0) nanotube capped (a) with a conical-shape tip (model I) and (b) with a conical joint containing a pentagon-heptagon pair reducing the diameter from 2 to 0.8 nm (model II). The horizontal bars indicate the zero-density levels. The Fermi level is at zero energy. The LDOS curves are averaged over the atoms (black spheres) composing the surface areas labeled by *A*, *B*, *C*, and *D*, as indicated by the corresponding letters in the right-hand side projection of both structures. Curve *A* corresponds to an LDOS averaged over a section of a cylindrical (24, 0) nanotube well below the tip region as indicated by the broken line. A resonant state associated with the tip apex appears for both structures (curve *D*), as well as an acceptor state (shown by arrows) in a small region containing the pentagon defect and its five adjacent hexagons.

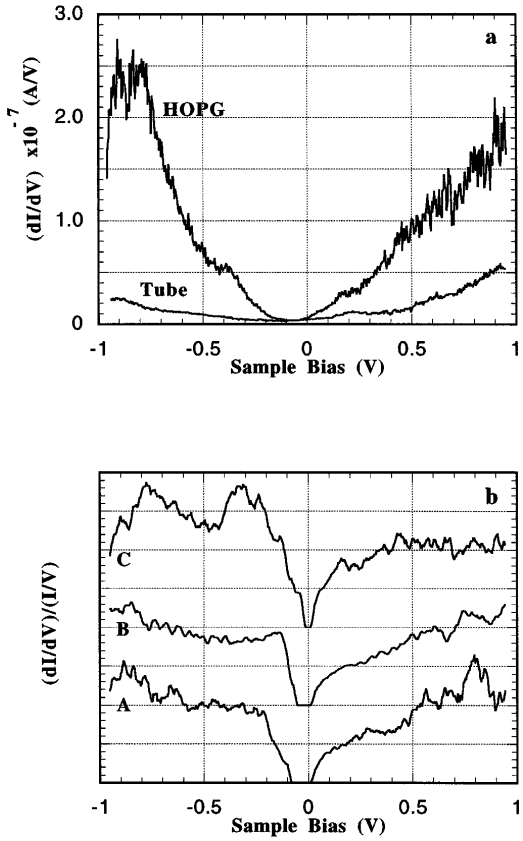

FIG. 3. Comparisons of electronic properties at the tube end and along its body, far from the end, for a 10 nm tube closed with a hemispherelike end. (a) The differential conductance is shown, as derived from tunneling spectra by numerical differentiation, for the HOPG substrate and the tube body. (b) The LDOS derived from the tunneling spectra is compared for the tube body (*A*) the tube end (*B*) and for the HOPG substrate (*C*). The conduction band is shown to the right of the Fermi level and the *Y*-axis units for LDOS plots are arbitrary.

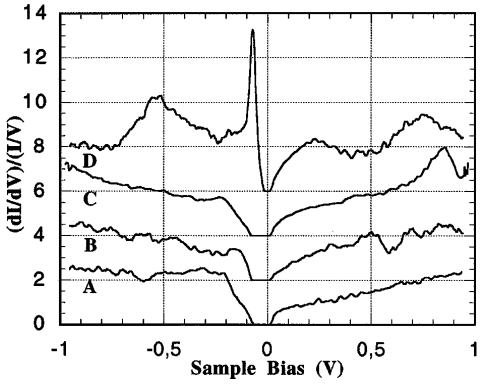

FIG. 4. Comparisons of the LDOS for the conical closure structure of the 20 nm tube. LDOS derived from the tunneling spectra acquired at the positions marked in Fig. 1(b) are presented. The spectra were recorded along the body of the tube (*A*), at the kink that begins the cone (*B*), half way between the beginning of the cone and its apex (*C*) and at the apex (*D*).

in the tubes. The LDOS [Fig. 3(b)] at the tube middle (*A*) and the tube end (*B*) are similar in the conduction band. For both cases a broad peak is observed around 0.8 eV. However, the valence band shows differences between tube middle and tube end. The shoulder which occurs at 100 meV from the Fermi level in the LDOS of the tube end is indicative of localized acceptor states. This state closes the apparent band gap from 100 meV at the middle to 70 meV on the end, suggesting that it is positioned within the band gap and overlaps with the band edge.

The effect of confinement on defect states is strikingly illustrated in the LDOS of the conically shaped closed ends, where defects are concentrated in a smaller volume. Figure 4 compares LDOS at four positions along the conical closure. The electronic structure in the conduction band from position to position along the cone shows only a slight, broad enhancement in the LDOS at the cone apex. In contrast to the conduction states, the valence band alters considerably. The LDOS from position *B* [marked on Fig. 1(b)] exhibits a shoulder at the valence band edge [100 meV from the Fermi level, as in Fig. 3(b)]. Position *B* is related to the introduction of a single pentagon and a possible shift in the chirality of the lattice to form the cone. The LDOS at *C*, which lies far from the position of the pentagon at *B*, does not show this state, but shows a slight increase in the overall LDOS at 200 meV from the Fermi level. The LDOS at *D* is the most striking with the valence state greatly enhanced and increasing in the overall electron state density at both valence and conduction band edges. The increased confinement of defects at the cone apex has produced very sharp resonant states, in the valence band edge, which is considerably more enhanced in comparison to the states observed from the end region of the 10 nm tube [Fig. 3(b)]. The states disappear within a spatial extent of 25.0 nm, which was the closest separation of tunneling spectra acquired.

At low voltages it is expected that the STM is most sensitive to the electronic structure of the outermost tube layer. The relatively large diameter of the tubes further rules out ballistic transport to the substrate. Moreover, the fact that we find similar LDOS at different positions of a tapering cone (it is inevitable that as we go from *A* and *D* [Fig. 1(b)] the number of layers should decrease) suggests that the main contribution to LDOS comes only from the outermost layer of the tube.

To understand the relation between topology and electronic properties at the tips of nanotubes, we perform simple tight-binding studies of different tube end structures (Fig. 2) chosen to mimic the outermost layer of the conical structure reported in Fig. 1(b). The model is restricted to π-π^* orbitals only, and we adopt a recursion technique in order to account properly for the semi-infinite geometry of the capped nanotubes [13]. We construct a $(24, 0)$ nanotube (2 nm diameter) [14], capped in two different ways (models I and II in Fig. 2). In model I, a hexagon is placed on the top of the tip apex and the conical shape of the tip is obtained by displacing one of the six pentagons to *B*, thus breaking the threefold symmetry. In model II, a pentagon-heptagon pair is used to connect the

(24, 0) nanotube to a (10, 0) nanotube capped by a hemispherical tip apex containing six pentagons in a fivefold symmetric arrangement.

The curves on the left-hand side of Figs. 2(a) and 2(b) are the π-π^* LDOS averaged over (*A*) a belt of hexagons far from the tip, (*B*) a region containing the first pentagon, (*C*) a portion of the conical region, and (*D*) the tip apex, to allow for direct comparison of the experimental data provided in Fig. 4. In the two models, the *A*, *B*, and *C* LDOS are very similar. The *B* LDOS shows the appearance of acceptor states (shown by arrows) located just above the top of the valence band edge. This is related to the presence of a pentagon in region *B*, in agreement with the present experimental observations (Fig. 4), and previous theoretical works [13,15]. In addition, we observe strong and sharp peaks (see *D* LDOS) associated with the electronic states localized at the tip apex, consistent with a previous theoretical paper [7]. As evidenced in Fig. 2, different tip apex topologies can yield donor or acceptor states. The agreement between the LDOS of model II and that observed experimentally (Fig. 4) is consistent with a conical-joint geometry common to the two systems depicted in Figs. 1(b) and 2(b). We find, however, that a conical-shape cap derived from the tip apex topology of model II leads to a peak in the valence region (although less sharp). This indicates that the relative position of pentagons in the tip apex is more important than the global shape of the cap to determine the position of the localized states. We note that the tip apex diameter of model II (0.8 nm) is relatively small compared to experiment (2 nm). Indeed, if we consider a tip made of a (20, 0) nanotube (1.6 nm of diameter) capped by half a C_{240} instead of the (10, 0) nanotube capped by half a C_{60} as in model II, we find a localized state peak at $\sim$0.4 eV below the Fermi level, improving the agreement of Fig. 2(b) with experiment. Increasing the diameter of the tip apex also results in a broadening of the peak, presumably due to a reduced confinement of the pentagons. This may explain why Fig. 3(b) (tip apex diameter $\sim$20 nm) exhibits a broad shoulder at the valence band edge rather than a sharp peak as in Fig. 4 (tip apex diameter $\sim$2 nm).

In conclusion, STS and tight-binding calculations have been used to identify local variations of electronic structure in carbon nanotubes and their tips. Our results provide the first experimental evidence for the presence of sharp resonant states near the valence band edge in the LDOS of carbon nanotubes. The energy and the strength of these resonances can be correlated to interacting pentagonal coordinated defects and their density. Further, the introduction of isolated pentagonal defects in the nanotube lattice is seen to result in weak acceptor states.

P. M. A. acknowledges the Alexander von Humboldt Stiftung for financial support. P. M. A., D. L. C., and P. R. thank Professor Dawn Bonnell for discussions and Professor Manfred Rühle for encouragement. J. C. C. is indebted to the National Fund for Scientific Research of Belgium and EEC Grant of the Human Capital and Mobility project for financial supports. J. C. C., A. D. V., X. B., and R. C. acknowledge support from the Swiss NSF and from the PATP collaborative project between Cray Research, Inc. and EPFL. The authors acknowledge W. de Heer for discussion on the influence of tip states on field emission.

*Permanent address: Department of Physics and Astronomy, Clemson University, Clemson, South Carolina 29634.

†Permanent address: Department of Materials Science & Engineering, Rensselaer Polytechnic Institute, Troy, New York 12180-3590.

‡Permanent address: Université Catholique de Louvain, Unité PCPM, Place Croix du Sud 1, B-1348 Louvain-la-Neuve, Belgium.

§Permanent address: Département de Physique Matériaux, Université Claude Bernard, 43 bd. du 11 Novembre 1918, F-69622 Villeurbanne Cedex, France.

[1] M. Dresselhaus, G. Dresselhaus, and P. C. Eklund, *Science of Fullerenes and Carbon Nanotubes* (Academic Press, San Diego, 1996); *Carbon Nanotubes, Preparation and Properties*, edited by T. W. Ebbesen (CRC Press, New York, 1996).

[2] S. Iijima and T. Ichihashi, Nature (London) **363**, 603 (1993); D. S. Bethune *et al.*, Nature (London) **363**, 605 (1993); A. Thess *et al.*, Science **273**, 483 (1996).

[3] S. Iijima, Nature (London) **354**, 54 (1991); T. W. Ebbesen, Phys. Today **49**, No. 6, 26 (1994).

[4] M. M. J. Treacy, T. W. Ebbesen, and J. M. Gibson, Nature (London) **381**, 678 (1996).

[5] T. W. Ebbesen, H. J. Lezec, H. Hiura, J. W. Bennet, H. F. Ghaemi, and T. Thio, Nature (London) **382**, 54 (1996); L. Langer *et al.*, Phys. Rev. Lett. **76**, 479 (1996); A. Y. Kasumov, I. Khodos, P. M. Ajayan, and C. Colliex, Europhys. Lett. **34**, 429 (1996).

[6] S. Iijima, T. Ichihashi, and Y. Ando, Nature (London) **356**, 776 (1992); P. M. Ajayan, T. Ichihashi, and S. Iijima, Chem. Phys. Lett. **202**, 384 (1993).

[7] R. Tamura and M. Tsukada, Phys. Rev. B **52**, 6015 (1995).

[8] W. A. de Heer, A. Chatelain, and D. Ugarte, Science **270**, 1179 (1995); A. G. Rinzler *et al.*, Science **269**, 1550 (1995); P. G. Collins and A. Zettl, Appl. Phys. Lett. **69**, 1969 (1996).

[9] W. A. de Heer, J.-M. Bonard, K. Fauth, A. Chatelain, L. Forro, and D. Ugarte, Adv. Mater. **9**, 87 (1997).

[10] W. Rivera *et al.*, J. Vac. Sci. Technol. B **13**, 327 (1995); K. Sattler, Carbon **33**, 915 (1995); Z. Zhang and C. M. Lieber, Appl. Phys. Lett. **62**, 2792 (1993); C. H. Olk and J. P. Heremans, J. Mater. Res. **9**, 259 (1994).

[11] T. W. Ebbesen and P. M. Ajayan, Nature (London) **358**, 220 (1992).

[12] R. M. Feenstra, in *Scanning Tunneling Microscopy and Related Methods*, edited by R. J. Behm, N. Garcia, and R. Rohrer (Kluwer, Boston, 1990).

[13] The technical details and reliability of this approach have been discussed in J.-C. Charlier, T. W. Ebbesen, and Ph. Lambin, Phys. Rev. B **53**, 11 108 (1996).

[14] In the notation of N. Hamada, S. I. Sawada, and A. Oshiyama, Phys. Rev. Lett. **68**, 1579 (1992).

[15] R. Tamura and M. Tsukada, Phys. Rev. B **49**, 7697 (1994).